PHYSICAL REVIEW B VOLUME 52, NUMBER 8 15 AUGUST 1995-II

Fluctuation effects on the electrodynamics of quasi-one-dimensional conductors above the charge-density-wave transition

A. Schwartz,* M. Dressel, B. Alavi, A. Blank, S. Dubois, and G. Grüner
Department of Physics, University of California, Los Angeles, Los Angeles, California 90024-1547

B.P. Gorshunov, A.A. Volkov, and G.V. Kozlov
Institute of General Physics, Russian Academy of Science, Moscow 117942, Russia

S. Thieme and L. Degiorgi
Laboratorium Festkörperphysik, Eidgenössische Technische Hochschule, CH-8093 Zürich, Switzerland

F. Lévy
Institut de Physique Appliquée, Ecole Polytechnique Fédérale de Lausanne, CH-1015 Lausanne, Switzerland

(Received 2 November 1994; revised manuscript received 27 February 1995)

The complex conductivity spectra of the quasi-one-dimensional compounds $K_{0.3}MoO_3$ (blue bronze) and $(TaSe_4)_2I$ in the conducting phase (above T_{3D} = 183 K and 263 K, respectively, but below the mean-field temperature T^{MF}) have been measured over a broad frequency range, 1–10^5 cm^{-1}, using a combination of different spectroscopic techniques; we have also investigated the effects of disorder. Clearly pronounced excitations are discovered in the spectra below 50 cm^{-1} for the electric field $\vec{E}$ parallel to the chains, the direction along which the charge-density wave develops below the Peierls transition temperature T_{3D}. We associate these excitations with charge-density-wave fluctuations that exist even at room temperature and result in a collective contribution to the conductivity. For the transverse polarization, $\vec{E}$ perpendicular to the chains, no such low-frequency excitations are evident in the conductivity spectra. These measurements give clear evidence for important deviations from conventional metallic behavior in the fluctuating region below T^{MF} but above T_{3D}, the temperature where three-dimensional long-range order develops.

I. INTRODUCTION

Ever since the discovery of materials with strongly anisotropic properties,[1–4] it has been recognized that fluctuation effects play an important role above the three-dimensional ordering transition T_{3D} in quasi-one-dimensional systems. The mean-field solution of an ideal one-dimensional system leads to a finite transition temperature T^{MF} where long-range order develops and the system undergoes a Peierls transition to a charge-density-wave (CDW) ground state.[5,6] This, however, is an artifact of the mean-field approximation, which neglects the role played by fluctuations of the order parameter. On the contrary, a strictly one-dimensional system with only short-range interactions does not develop long-range order at finite temperature.[7] Real quasi-one-dimensional materials, however, are highly anisotropic three-dimensional systems with interchain electronic Coulomb interactions and tunneling leading to coupling of the fluctuations that develop along each chain. This coupling results in a finite transition temperature T_{3D} below which three-dimensional long-range order occurs. For weak interchain coupling, T_{3D} is significantly smaller than T^{MF}. The region below T^{MF} is characterized by one-dimensional fluctuations which, at some temperature $T^* > T_{3D}$, cross over to fluctuations with two- or three-dimensional character. T^* is the temperature at which the transverse correlation length $\xi_\perp$ becomes comparable to the interchain spacing. Figure 1 shows a schematic overview of the different temperature ranges.

The mean-field transition temperature T^{MF} can be estimated from the value of the CDW gap in the $T \to 0$ limit using the well-known relation[6] $\Delta = 1.764 k_B T^{MF}$, and the gap Δ can be calculated from a fit to the activated behavior of the dc conductivity below the metal-insulator transition temperature T_{3D}. It can also be found by low-temperature infrared reflectivity measurements, or from the extrapolation of scattering results and susceptibility experiments. The results of these evaluations are listed in Table I. In the accompanying publication[14] we discuss the spectral features below T_{3D}, with a focus on thermal lattice fluctuations. The present paper focuses on fluctuation effects that occur above T_{3D}.

A number of experimental results, such as x-ray and neutron scattering, magnetic susceptibility, and optical reflectivity, give evidence that such fluctuation effects play an important role for the electrodynamics of inorganic linear chain compounds, such as $K_{0.3}MoO_3$ and $(TaSe_4)_2I$, in the temperature range above the CDW transition. Fluctuation effects well above the three-dimensional Peierls transition have been clearly observed by scattering[15] and magnetic susceptibility[8,10] measurements.

©1995 The American Physical Society

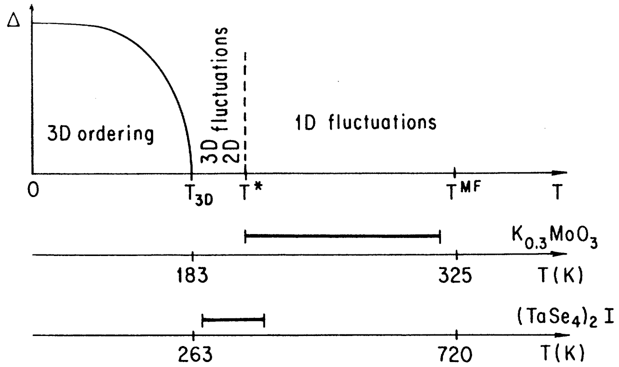

FIG. 1. The various temperature regimes in the behavior of a one-dimensional conductor. T^{MF} indicates the mean-field temperature as derived from the temperature dependence of the susceptibility, the optical response, or the activation energy of the dc conductivity. Upon lowering the temperature below T^{MF}, first one-dimensional fluctuations start to occur; below T^* these change over to two- and three-dimensional fluctuations. $T_{3\mathrm{D}}$ is the actual temperature of the Peierls transition, where three-dimensional ordering starts and the gap as the order parameter begins to increase. We also indicate the temperature range where the experiments reported here were performed. While we span a wide range of temperatures between T^* and T^{MF} in the case of $\mathrm{K_{0.3}MoO_3}$, due to the high transition temperature of $\mathrm{(TaSe_4)_2I}$, our measurements on this compound always stay close to $T_{3\mathrm{D}}$.

In view of these results it is interesting to ask how CDW fluctuations influence electronic transport properties and the excitation spectrum in this class of materials. Earlier reflectivity measurements[9,11,16–19] on $\mathrm{K_{0.3}MoO_3}$ and $\mathrm{(TaSe_4)_2I}$ show indications of a gap at temperatures slightly above $T_{3\mathrm{D}}$ in both compounds. This gap steadily develops upon further cooling, and the $T \rightarrow 0$ values are listed in Table I. Previously, however, experimental limitations of IR reflectivity measurements precluded a detailed study of the low-frequency behavior, and the extrapolation necessary in order to meet the dc data was always speculative. The excitation spectra obtained by Kramers-Kronig[20] analysis therefore contained large uncertainties, especially at low frequencies.

It has also been suggested that in such low-dimensional materials deviations from Fermi liquid behavior may occur, and that models such as the Luttinger liquid may be more appropriate.[21,22] This hypothesis is supported by high-resolution photoemission experiments[23] on $\mathrm{K_{0.3}MoO_3}$ and $\mathrm{(TaSe_4)_2I}$, which above $T_{3\mathrm{D}}$ do not show the sharp Fermi edge characteristic of conventional three-dimensional metals. The absence of a metallic step in one-dimensional systems may be an indication of a pseudogap, which appears in the temperature range $T_{3\mathrm{D}} < T < T^{\mathrm{MF}}$ as a result of fluctuations and leads to a strong reduction of the spectral intensity near the Fermi edge. However, from this explanation a temperature dependent evolution of the spectral intensity at the Fermi energy is expected and metallic behavior should be observed close to and above T^{MF}. No such sharp edge can be seen up to 300 K in either compound.[24] Although this is in agreement with the continuous increase of the susceptibility[8,10] in this range, Dardel *et al.*[24] suggest that their observations are an indication that the one-dimensional metals are not well described by the standard Fermi liquid model but should instead be seen as marginal Fermi liquids or Luttinger liquids, both of which also have a reduced density of states at the Fermi level. The calculations of the Luttinger model, however, assume a strictly one-dimensional system, which is certainly not the case. The Luttinger liquid may be unstable for finite interchain coupling,[21] but there is currently no agreement on extension of the model to include higher-dimensional effects.

This paper reports on our detailed studies of the electrodynamic response of the one-dimensional metals $\mathrm{K_{0.3}MoO_3}$ and $\mathrm{(TaSe_4)_2I}$ in the temperature range above $T_{3\mathrm{D}}$ but below T^{MF}. Although our experiments do cover a broad spectral range (1–10^5 cm^{-1}), we will focus in particular on the frequency range below the single-particle gap, which has not been previously studied at these temperatures, and which besides the effects of the pseudogap contains important collective contributions to the conductivity. Some of our results have been published earlier.[25,26]

TABLE I. The value of the single-particle gap at $T = 0$ K as determined from the activation energy of the low-temperature resistivity, from the temperature dependence of the susceptibility, from optical measurements at low temperatures, and from neutron and Raman scattering experiments. The long-range charge-density-wave ordering temperature $T_{3\mathrm{D}}$ for $\mathrm{(TaSe_4)_2I}$ and $\mathrm{K_{0.3}MoO_3}$ is determined from transport and thermodynamic measurements; the approximate mean-field temperature T^{MF} is obtained from the activation energy by $1.76 k_B T^{\mathrm{MF}} = \Delta_\chi$. The Pauli susceptibility χ^{Pauli} was determined from the high-temperature extrapolation of the magnetic susceptibility data.

	Δ_ρ (cm^{-1})	Δ_χ (cm^{-1})	Δ_{opt} (cm^{-1})	$\Delta_{\mathrm{scatter}}$ (cm^{-1})	$T_{3\mathrm{D}}$ (K)	T^{MF} (K)	χ^{Pauli} (10^{-6} cm^3/mole)
$\mathrm{(TaSe_4)_2I}$	1200	890[a]	1610[b]		263	720	20.2[a]
$\mathrm{K_{0.3}MoO_3}$	350	400[c]	600[d]	210[e]	183	325	24.1[c]

[a] Johnston *et al.*, Ref. 8.
[b] Berner *et al.*, Ref. 9.
[c] Johnston, Ref. 10.
[d] Travaglini *et al.*, Ref. 11.
[e] Pouget *et al.*, Ref. 12; and Travaglini *et al.* Ref. 13.

II. EXPERIMENTAL TECHNIQUES AND RESULTS

Single crystals of $(TaSe_4)_2I$ were grown using vapor transport. The stoichiometric mixture of the high-purity constituents was sealed in an evacuated quartz tube, and the reaction performed in a gradient furnace with a typical temperature gradient of 10 °C/cm. The crystals formed near the cold end of the tube, and over the crystal growth region the temperature varied between 450 °C and 530 °C. Large crystals of up to $10 \times 4 \times 1$ mm^3 grew within a period of three days. For our optical experiments, we polished the surface to a flatness of better than 1 μm.

The $K_{0.3}MoO_3$ crystals used in this study were grown by electrolytic reduction of a molten mixture of K_2MoO_4 and MoO_3. The successful crystallization is dependent upon the reduction temperature and the moderation of K_2MoO_4 to MoO_3. In order to prepare $K_{0.3}MoO_3$, we used a simple electrolytic cell and employed platinum electrodes. Calcinated K_2MoO_4 was ground with MoO_3 in a ratio of 1:3.35 to 1:3.5, and the mixture was melted around 550 °C and poured into a Pyrex glass. This mixture was then ground coarsely and placed in the electrolytic cell, where it was remelted around 560 °C. The electrolysis is usually performed at low currents (10–20 mA) and crystals formed on the cathode are periodically harvested. We also studied tungsten(W)-alloyed crystals grown by the same technique. Doping with WO_3 yields crystals in which the W concentration varies widely, but doping with K_2WO_4 results in a nearly uniform impurity distribution, as confirmed by electron microprobe analysis. The crystals can reach more than $10 \times 10 \times 3$ mm^3. For our optical studies, we used a pure $K_{0.3}MoO_3$ crystal with a surface of 10×8 mm^2 and a $K_{0.3}Mo_{0.996}W_{0.004}O_3$ single crystal, which had an 8×5 mm^2 surface. Both samples were carefully polished until the surface flatness was better than 1 μm. We tested the surface quality by looking at the Newton rings between the sample and a microscope slide, and we were, in general, able to reduce it to one ring over the face of the sample.

Figure 2 shows the temperature dependence of the dc conductivities of the three materials discussed above, measured by a standard four-wire technique. In all cases the absolute values are an average of various batches. At room temperature the parallel-chain conductivity of $(TaSe_4)_2I$ is (270 ± 60) $(\Omega\,\mathrm{cm})^{-1}$; perpendicular to the stacks we estimate $\sigma_\perp(300\ \mathrm{K}) \approx 4.0$ $(\Omega\,\mathrm{cm})^{-1}$ from our optical measurements. With decreasing temperature, the conductivity decreases even above T_{3D}=263 K. The anisotropy of the system remains unchanged with temperature in the range of interest (270 - 300 K).

The room-temperature conductivity of $K_{0.3}MoO_3$ [Fig. 2(b)] is (1500 ± 500) $(\Omega\,\mathrm{cm})^{-1}$ along the chain direction. Significantly different values were found even within one batch. It increases to 2000 $(\Omega\,\mathrm{cm})^{-1}$ at 200 K indicating the metallic nature of $K_{0.3}MoO_3$; the anisotropy $\sigma_\parallel/\sigma_\perp$ is 30 at both temperatures, in agreement with earlier reported findings.[27] Both ratios $\sigma_\parallel/\sigma_\perp$ and $\sigma(200\ \mathrm{K})/\sigma(300\ \mathrm{K})$ are sample independent even though the absolute value of conductivity is not. Doping the crystals with 0.4% tungsten does not change the high-temperature dc conductivity significantly.

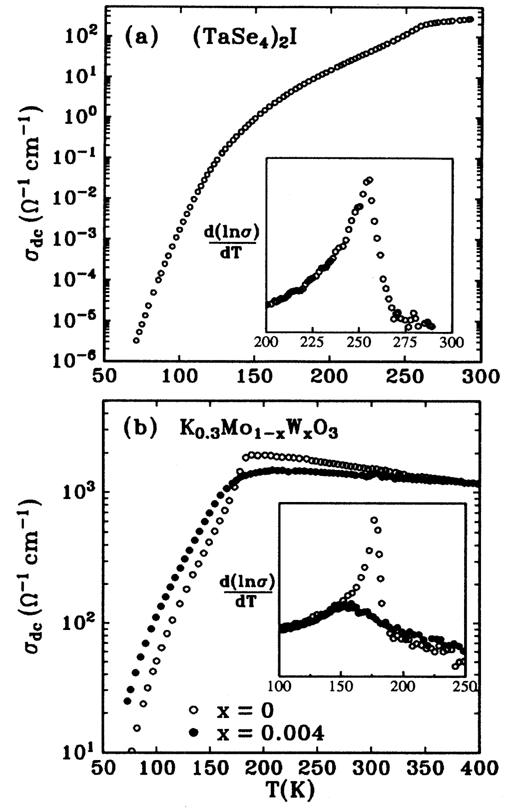

FIG. 2. Temperature dependences of the dc conductivities along the highly conducting axes of (a) $(TaSe_4)_2I$ and (b) of $K_{0.3}MoO_3$ and $K_{0.3}Mo_{0.996}W_{0.004}O_3$. The insets show the derivatives, which are used to determine the transition temperatures.

Various techniques have been employed to obtain the electrodynamic response in an extremely wide frequency range. In the microwave range, a cavity perturbation technique[28] was used to measure the surface impedance $\hat{Z}_S = R_S + iX_S$ at various temperatures. By placing a needle-shaped crystal in the maximum of the electric field of a cylindrical TE_{011} cavity ($f_0 = \omega/2\pi = \nu c =$ 7.4 GHz and 35.1 GHz) and measuring the change in width ($\Delta\Gamma$) and central frequency (Δf) of the resonance, it is possible to calculate both the surface resistance R_S and the surface reactance X_S:

$$R_S = Z_0 \frac{\Delta\Gamma}{2 f_0 \zeta} \quad , \qquad X_S = Z_0 \frac{\Delta f}{f_0 \zeta}, \tag{1}$$

where $Z_0 = 4\pi/c = 4.19 \times 10^{-10}$ s/cm is the free space impedance. [$Z_0 = 377\ \Omega$ in *Système International* units.] The resonator constant ζ can be calculated from the geometry of the cavity and the sample.[28–30] Similar data were taken at 100 GHz and 60 GHz by replacing the copper endplate of a rectangular TE_{103} cavity by the sample. Again, by measuring $\Delta\Gamma$ and Δf, this technique allows us to accurately determine the absolute value of the real and imaginary parts of the surface impedance of highly anisotropic conductors.[31] We were not able to determine the electrodynamic response in the perpendicular direction because the higher surface resistance results in a large broadening of the resonance.

The complex conductivity ($\hat{\sigma} = \sigma_1 + i\sigma_2$) and permittivity ($\hat{\epsilon} = \epsilon_1 + i\epsilon_2$) can be calculated from the surface impedance using $\hat{Z}_S = Z_0\sqrt{\nu c/2i\hat{\sigma}}$ and $\hat{\epsilon} = 1 + 2i\hat{\sigma}/\nu c$. In addition, the absorptivity A can be calculated using the relation

$$A = 1 - R = \frac{4R_S}{Z_0}\left(1 + \frac{2R_S}{Z_0} + \frac{R_S^2 + X_S^2}{Z_0^2}\right)^{-1}, \qquad (2)$$

where R is the reflectivity. At some frequencies (7.4, 35.1, and 60 GHz) our measurement of R_S was significantly more accurate than that of X_S, but since the materials are well in the limit $R_S, |X_S| \ll Z_0$, Eq. (2) can be simplified to

$$A \approx \frac{4R_S}{Z_0}. \qquad (3)$$

In order to evaluate σ_1 in this case, it was necessary to assume the Hagen-Rubens relation[32]

$$A = 2\left(\frac{\nu c}{\sigma_1}\right)^{1/2}, \qquad (4)$$

which is valid for $\sigma_1 \gg \nu c \epsilon_1$.

The relatively low conductivity of $(TaSe_4)_2I$ allowed for the use of a submillimeter (submm) complex transmission measurement technique.[33,34] The sample was polished to a thickness of about 10 μm, with the two surfaces parallel within parts of a micrometer over the optical face. The amplitude and phase shift of the transmitted radiation were measured and used to determine $\sigma_1(\nu)$ and $\epsilon_1(\nu)$, as well as the absorptivity A. With this technique, the complex response of $(TaSe_4)_2I$ was measured at room temperature and at 270 K, between 12 and 22 cm^{-1} for the electric field $\vec{E}$ parallel to the conducting c axis, and between 12 and 36 cm^{-1} for $\vec{E} \perp c$.

The conductivity of $K_{0.3}MoO_3$ along the chain direction is sufficiently high that even a 7-μm-thick sample is not transparent in the submm frequency range (transmission coefficient $< 10^{-5}$). Thus, at frequencies between 8 cm^{-1} and 36 cm^{-1}, we measured the reflectivity of crystals using the submillimeter spectrometer discussed above,[33] but rearranged for reflectivity measurements. The reflection coefficient was obtained by comparing the signals reflected from the sample and from a brass reference mirror, where the reflectivity of brass was calculated from the dc conductivity σ_{dc} by the Hagen-Rubens relation [Eq. (4)] since $\sigma_1 = \sigma_{dc}$ in this limit. The reflectivity of $K_{0.3}Mo_{0.996}W_{0.004}O_3$ was also measured in this manner.

In addition to reflectivity and transmission measurements, we employed a technique developed for direct measurements of $\epsilon_1(\nu)$ and $\sigma_1(\nu)$ of highly reflecting materials in this submm wave frequency range.[31,35,36] This technique is based on a Fabry-Pérot resonator formed by a plane-parallel radio-transparent dielectric plate (z-cut sapphire) and the bulk sample (with an optically flat surface of about 10×8 mm^2) in optical contact with its rear face. The reflectivity spectra of the resonator contain sharp interference fringes (minima) due to multiple reflections inside the plate. The highest sensitivity of this Fabry-Pérot resonator technique is realized at these resonance frequencies, where the interaction of the radiation with the sample is most effective. By comparing the parameters of the minima (central frequency and amplitude or Q factor) to those obtained with the sample replaced by a metallic mirror, it is possible to directly calculate both ϵ_1 and σ_1 of the sample.[31]

Employing this technique we measured ϵ_1 and σ_1 of a $K_{0.3}MoO_3$ single crystal at six frequencies between 8 and 36 cm^{-1}, at 300 K and 200 K, and for two principal orientations of $\vec{E}$ relative the conducting b axis, $\vec{E} \parallel b$ and $\vec{E} \perp b$ (i.e., $\vec{E} \parallel a + 2c$). Also, for $\vec{E} \perp b$, the lower conductivity allowed for transmission measurements on a specially prepared ca. 10-μm-thick sample, just as was done for the $(TaSe_4)_2I$. Both types of measurements led to identical results for ϵ_1 and σ_1 in the perpendicular direction, confirming the validity of this new Fabry-Pérot reflectivity technique. In addition, it is possible to evaluate the reflectivity R from this Fabry-Pérot measurement, and it is found to be in perfect agreement with the directly measured reflectivity discussed above.[31]

In the optical range from 14 cm^{-1} up to 10^5, standard polarized reflection experiments ($\vec{E}$ parallel and perpendicular to the chains) on $K_{0.3}MoO_3$, $K_{0.3}Mo_{0.996}W_{0.004}O_3$, and $(TaSe_4)_2I$ single crystals were performed by using four different spectrometers with overlapping frequency ranges. In the infrared spectral range, two Fourier transform interferometers were used with a gold mirror as a reference. In the far-infrared (FIR) we made use of a Bruker IFS113v Fourier transform interferometer with a Hg arc light source and a He-cooled Ge bolometer detector, while from the FIR up to the mid-infrared (MIR) a fast scanning Bruker IFS48PC spectrometer was used. Two grating spectrometers were employed at higher frequencies: a homemade spectrometer based on a Zeiss monochromator in the visible and a McPherson spectrometer in the ultraviolet.

In addition to the direct evaluation of σ_1 and ϵ_1 from the optical data as described above, a Kramers-Kronig analysis[20] of the reflectivity data was performed. There is some degree of uncertainty associated with this procedure, since it requires one to make some decisions about how to join the data from different measurements, and also how to extrapolate to low and high frequencies. Therefore, we chose to follow a different procedure, which allowed us to simultaneously consider A, σ_1, and ϵ_1 data. We fit the overall behavior of the data by a minimum set of harmonic oscillators and Drude terms necessary to describe all significant features observed in the conductivity, permittivity, and absorptivity spectra combined (including σ_{dc}):

$$\hat{\epsilon}(\nu) = \epsilon_1(\nu) + i\epsilon_2(\nu) = \epsilon_\infty + \sum_i \frac{\nu_{pi}^2}{\nu_{0i}^2 - \nu^2 - i\nu\gamma_i}, \qquad (5)$$

where ν_{0i}, ν_{pi}, and γ_i are the frequency, mode strength

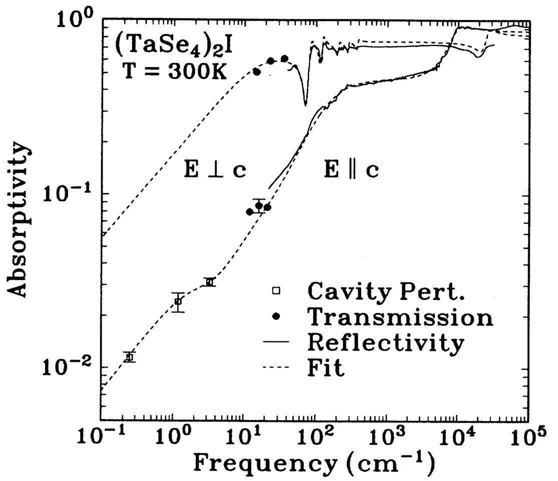

FIG. 3. Frequency dependence of the room-temperature absorptivity of $(TaSe_4)_2I$ in both orientations $\vec{E} \parallel c$ and $\vec{E} \perp c$. The open squares were obtained from the surface resistance, and the full circles calculated from quasioptical transmission measurements. The solid lines show the results of optical reflectivity experiments. The dashed lines show the dispersion analysis of the data, as described in the text.

or plasma frequency, and damping of the oscillators, respectively ($\nu_{0i} = 0$ describes a Drude term). Since we want to focus on the low-frequency behavior, excitations above ca. 10^4 cm^{-1} were summarized by an appropriate value of ϵ_∞.

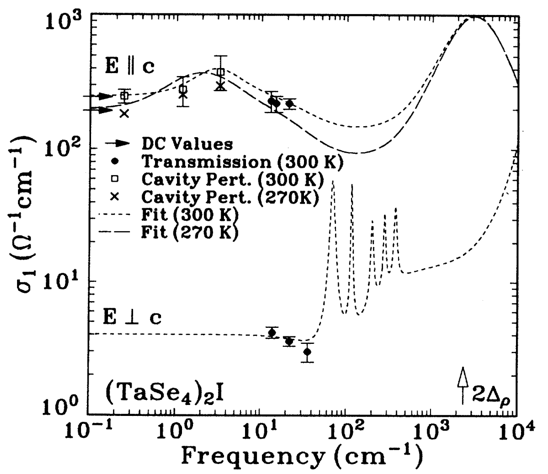

FIG. 4. Frequency dependence of the conductivity of $(TaSe_4)_2I$ for $\vec{E} \parallel c$ (T = 300 K, 270 K) and for $\vec{E} \perp c$ (300 K). The solid circles show the results of a direct measurement of the conductivity by submm wave transmission experiments at 300 K. The open squares and the crosses are calculated from the surface impedance measurements at T = 300 K and 270 K, respectively. The open arrow indicates the single-particle gap $2\Delta_\rho$ as calculated from a fit of the activated behavior of the low-temperature dc conductivity using Eq. (6). The short-dashed lines are the results of our dispersion analysis of the 300 K data in both orientations, while the long-dashed line is the fit to the data at 270 K. The dc conductivities are indicated by the solid arrows.

TABLE II. Parameters of the Drude-Lorentz model [Eq. (5)] used to fit the electrodynamic response of $(TaSe_4)_2I$ in the direction parallel to the chains. ν_0 is the center frequency of the oscillator ($\nu_0 = 0$ indicates a Drude term), ν_p is the plasma frequency or spectral weight, and γ is the width or damping of the oscillator; ϵ_∞ was taken to be 4.5.

270 K			300 K		
ν_0 (cm^{-1})	ν_p (cm^{-1})	γ (cm^{-1})	ν_0 (cm^{-1})	ν_p (cm^{-1})	γ (cm^{-1})
0	440	28	0	450	30
2	230	5	3	210	5
0	3000	1800	0	4150	2100
3200	18 940	6200	3200	18 790	6120

Figures 3 and 4 present the absorptivity and conductivity data obtained on $(TaSe_4)_2I$, along with the results of the dispersion analysis, and the fit parameters are in Table II; Figures 5 and 6 show the analogous data for $K_{0.3}MoO_3$, with the parameters given in Table III. For both compounds, our results in the IR range are essentially the same as those obtained previously[9,11,17–19,37] and we will therefore focus the subsequent discussion on the lower frequency data and the new features that appear in the spectra below ca. 100 cm^{-1}. It is seen that in both compounds the conductivity increases at low frequency, and there is a maximum near 2–3 cm^{-1}, the strongest evidence for this peak coming from the absorptivity data, which show a clear change of slope in the region from 1–10 cm^{-1}. Since the microwave cavity technique is able to measure R_S more accurately than X_S, we weighted our analysis to the A data, which are basically independent of X_S [Eq. (3)]. This inflection in A leads to the maximum in σ_1. In all cases, the first two terms presented in Tables II and III are associated with

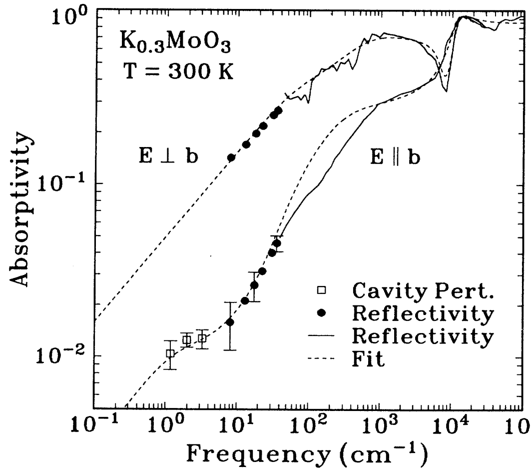

FIG. 5. Frequency dependence of the room-temperature absorptivity of $K_{0.3}MoO_3$ in both orientations $\vec{E} \parallel b$ and $\vec{E} \perp b$. The open squares were obtained by measuring the surface resistance, the solid circles represent data of quasioptical reflectivity measurements. The solid lines show the optical reflectivity data. The dashed lines show the results of the dispersion analysis of the data. We did not try to describe the large number of phonon features which can be seen in the perpendicular direction.

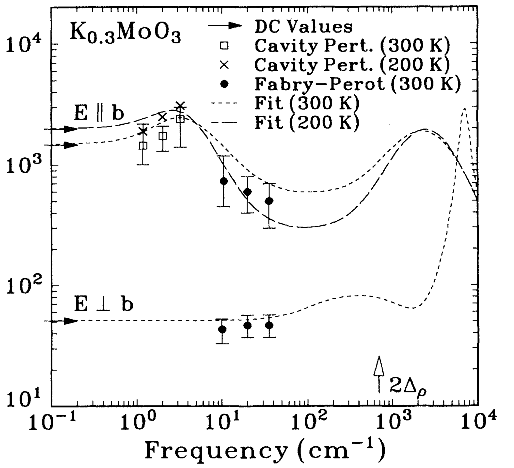

FIG. 6. Frequency dependence of the conductivity of $K_{0.3}MoO_3$ for $\vec{E} \parallel b$ (T = 300 K, 200 K) and for $\vec{E} \perp b$ (300 K). The solid points show the result of a direct measurement of the conductivity by the Fabry-Pérot reflectivity technique, and the open squares are calculated from the surface impedance measurements. The dashed lines represent the dispersion analysis of the entire data set. The open arrow indicates the single-particle gap $2\Delta_\rho$ as determined by fitting Eq. (6) to the low-temperature dc conductivity. The solid arrows show the dc conductivities.

this new feature, and the second two terms account for single-particle contributions to the conductivity. Later we will show that the low-frequency behavior can be described by a single term, and that it is a result of the collective behavior of the CDW fluctuations.

Figures 7 and 8 compare the absorptivity and conductivity spectra of $K_{0.3}Mo_{0.996}W_{0.004}O_3$ to those of the undoped material; the parameters of the dispersion analysis are compared in Table III. The introduction of defects to $K_{0.3}MoO_3$ changes the transition temperature to $T_{3D} \approx 150$ K as determined by dc conductivity and susceptibility[38] measurements. As shown in the inset of Fig. 2(b), the transition is broadened significantly. In addition, the activation energy at low temperatures seems to decrease slightly with higher doping concentration. However, at room temperature we do not see a significant change in the optical properties above 200 cm^{-1}. At 300 K, the absolute value of the dc conductivity of the alloyed sample is slightly lower than that of the pure $K_{0.3}MoO_3$ as seen in Fig. 2(b). The low-lying excitation is reduced in height (lower dc conductivity), resulting in a lower spectral weight of the narrow Drude-like feature.

III. DISCUSSION

The electrodynamic responses of $K_{0.3}MoO_3$ and $(TaSe_4)_2I$ clearly exhibit similar overall behavior, indicating that these features are related to the general properties of quasi-one-dimensional conductors with a CDW ground state. They show an extremely anisotropic response connected with the one-dimensional nature of the charge transport. While $(TaSe_4)_2I$ (Fig. 3) has a plasma edge at around 9000 cm^{-1} in the parallel direction ($\vec{E} \parallel c$), the absorptivity perpendicular to the chains is essentially frequency independent above 50 cm^{-1}, except for various phonon lines, and the reflectivity remains high, indicative of a large dielectric constant. Below 20 cm^{-1}, the conductivity perpendicular to the chains, $\sigma_\perp$, shows no dispersion, except for the wings of the phonon related features around 100 cm^{-1}, and can be well described by the Drude model, in spite of the low absolute value of $\sigma_\perp$(300 K). Although we are not aware of any dc measurement of the absolute value of $\sigma_\perp$, we estimate that $\sigma_\perp \approx 4.0$ $(\Omega\,\mathrm{cm})^{-1}$, giving an anisotropy of 60. The behavior of $K_{0.3}MoO_3$ is similar. Apart from phonon peaks, which we have not fit in detail, the conductivity perpendicular to the b direction, $\sigma_\perp$, is frequency independent below the submm frequency range, and $\sigma_\perp(T = 300\text{ K}) \approx 50$ $(\Omega\,\mathrm{cm})^{-1}$ at these frequencies, approximately equal to the dc value,[27] corresponding to the Hagen-Rubens behavior [Eq. (4)]. In $K_{0.3}MoO_3$, we find an anisotropy $\sigma_\parallel/\sigma_\perp$ of approximately 30, half that of the $(TaSe_4)_2I$, in agreement with the more one-dimensional nature of the latter compound.

Parallel to the chain direction, the conductivity spectra of both compounds display a gap related feature, as evidenced by the maximum of σ_1 above 1000 cm^{-1}. Below these maxima, the excitation spectra show two overall features: decreasing conductivity with decreasing frequency in the FIR range, and an enhanced conductivity at very low frequencies. These are clear deviations from a free carrier behavior, which would lead to a frequency independent conductivity up to the scattering rate $1/\tau$.

TABLE III. Parameters of the Drude-Lorentz model [Eq. (5)] used to fit the electrodynamic response of $K_{0.3}MoO_3$ and $K_{0.3}Mo_{0.996}W_{0.004}O_3$ in the direction parallel to the chains. The center frequency of the harmonic oscillators is given by ν_0 ($\nu_0 = 0$ indicates a Drude term), the plasma frequency or spectral weight is ν_p, and γ is the damping; ϵ_∞ was taken to be 5.0.

$K_{0.3}MoO_3$						$K_{0.3}Mo_{0.996}W_{0.004}O_3$		
200 K			300 K			300 K		
ν_0 (cm^{-1})	ν_p (cm^{-1})	γ (cm^{-1})	ν_0 (cm^{-1})	ν_p (cm^{-1})	γ (cm^{-1})	ν_0 (cm^{-1})	ν_p (cm^{-1})	γ (cm^{-1})
0	720	5	0	820	12	0	640	12
3.3	700	6.5	3.3	630	6.5	3.3	530	6.5
0	4100	1000	0	8000	1900	0	8100	1900
2500	25 100	5500	2500	24 550	6000	2500	24 620	6000

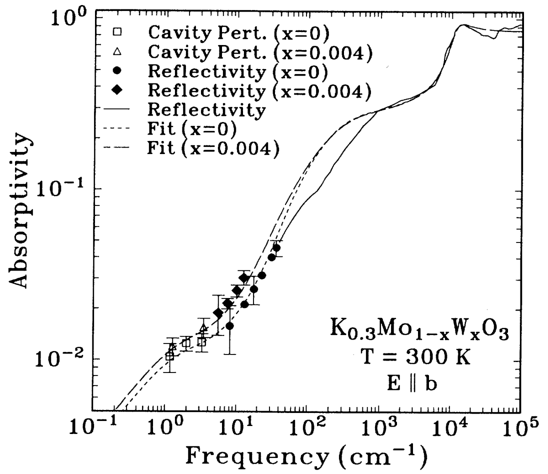

FIG. 7. The effect of doping is shown by the frequency dependence of the room-temperature absorptivities of $K_{0.3}Mo_{0.996}W_{0.004}O_3$ and $K_{0.3}MoO_3$. The open squares and triangles were obtained by measuring the surface resistance, the solid circles and diamonds represent data of quasioptical bulk reflectivity measurements. The solid line shows the optical results, which are essentially identical for this low-doping concentration. The dashed lines show the results of the dispersion analysis of the data for both compounds.

If we naively assume that all of the conduction electrons contribute individually to the dc conduction along the chain direction, then we obtain $\sigma_{\|} = (n_0 e^2 \tau / m_b)$, with $n_0 = 5.4 \times 10^{21}$ cm^{-3} the total electron density, e the electronic charge, and $m_b = 0.9 m_e$ the band mass[11] of $K_{0.3}MoO_3$. This yields $\gamma = (2\pi c \tau)^{-1} = 6000$ cm^{-1}, and the conductivity would be expected to be frequency independent well below this frequency. Instead, $\sigma_1(\nu)$ decreases with decreasing frequency for $\nu < 1000$ cm^{-1}. Due to the smaller dc conductivity, band mass ($m_b = 0.4 m_e$), and carrier concentration[18] ($n_0 = 3.2 \times 10^{21}$ cm^{-3}), the scattering rate of $(TaSe_4)_2I$ in this oversimplified picture is expected to be even higher: $\gamma = (2\pi c\tau)^{-1} \approx 45\,000$ cm^{-1}. The single-particle contribution at low frequencies is therefore small, with an upper limit in $K_{0.3}MoO_3$, for example, given by $\sigma_{\|} \approx 500$ $(\Omega\,\mathrm{cm})^{-1}$, measured around 100 cm^{-1}. Below T_{3D} the temperature dependent dc conductivities of both compounds show an activated behavior:

$$\sigma_{\mathrm{dc}} = \sigma_0 \exp\left\{ -\frac{\Delta}{k_B T} \right\} , \qquad (6)$$

with $2\Delta/hc \approx (700 \pm 100)$ cm^{-1} for $K_{0.3}MoO_3$ and (2400 ± 250) cm^{-1} for $(TaSe_4)_2I$. A comparison of these values to those obtained from other measurements is given in Table I.

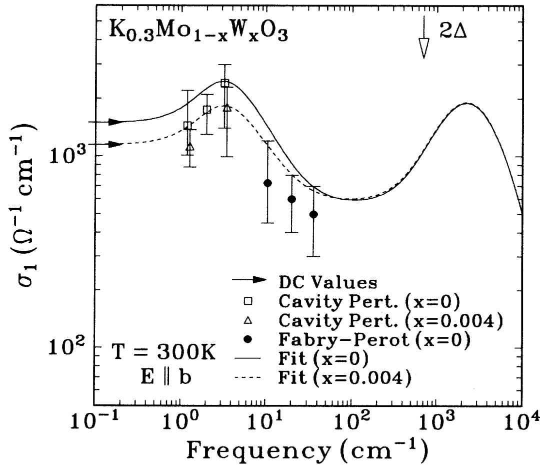

FIG. 8. Frequency dependence of the conductivity of $K_{0.3}Mo_{0.996}W_{0.004}O_3$ and pure $K_{0.3}MoO_3$ at room temperature. The solid points show the result of a direct measurement of the conductivity by a Fabry-Pérot technique. The open boxes and triangles are obtained from microwave surface impedance studies, while the solid arrows show the values of the dc conductivities. The single-particle gap $2\Delta_\rho$ obtained from the activated behavior of dc conductivity measurements on pure $K_{0.3}MoO_3$ crystals is indicated by the open arrow. The solid line represent the fit of the pure compound while the dashed line fits the doped $K_{0.3}Mo_{0.996}W_{0.004}O_3$.

Both compounds also show a pronounced low-frequency enhancement of $\sigma_{\|}$ at temperatures above T_{3D}. This implies an additional contribution to the conductivity in the $K_{0.3}MoO_3$ spectra for $\vec{E} \parallel b$ with a characteristic frequency $\nu_c \lesssim 10$ cm^{-1}; in the case of $(TaSe_4)_2I$ $\nu_c \lesssim 20$ cm^{-1} (see Figs. 4 and 6). Another clear indication of this mechanism comes from the frequency dependence of ϵ_1 in the submm wave range (Fig. 3 of Ref. 25). This is the result of the fluctuating CDW's, which give an additional contribution σ^* to the overall conductivity $\sigma_1 = \sigma^* + \sigma^{\mathrm{sp}}$, where σ^{sp} is the single particle conductivity. The collective contribution σ^* has two important features: finite dc conductivity and a small peak at 2 and 3 cm^{-1} for $(TaSe_4)_2I$ and $K_{0.3}MoO_3$, respectively. For both, this peak appears at about the same frequency where the pinned CDW resonance[39] occurs well below T_{3D}, and it arises in the fluctuation region as well due to the interaction of the fluctuating CDW segments with impurities.

We suggest that the features observed at low frequencies are due to the phase fluctuations of the electrons condensed into correlated CDW segments, with finite correlation length ξ along the chain direction. We assume that the CDW segments are locally pinned by impurity potentials but can, due to thermal fluctuations, be depinned and move diffusively. This admittedly crude picture explains two important features: the resonance at a finite frequency (the same as the pinned mode frequency in the ordered region) and the observation of finite dc conductivity.

The fluctuating CDW segments can be described using a model which was first developed in the context of the theory of Brownian motion[40,41] and has since been employed to describe the conductivity of superionic conductors.[42–44] We consider a system of particles, the CDW segments, moving in the presence of a weak periodic potential provided by impurities such that they exhibit both diffusive and oscillatory motion. The equation of motion can be written in the form of the generalized

Langevin equation based on a memory function formalism

$$m\ddot{x}(t) + m\Gamma_0\dot{x}(t) + m\omega_0^2 \int_{-\infty}^{t} M(t-t')\dot{x}(t')dt' = -eE(t)\ , \quad (7)$$

where $M(t)$ is a memory function. We assume that $x(t), E(t) \sim \exp\{-i\omega t\}$, and choose the form of M such that for large ω we obtain oscillatory motion

$$m\ddot{x} + m\Gamma_0\dot{x} + m\omega_0^2 x = -eE,$$

and for $\omega \to 0$ the system is diffusive

$$m\ddot{x} + m\gamma\dot{x} = -eE.$$

The simplest form of $M(t)$ that satisfies these conditions is $M(t) = \exp\{-t/\tau_c\}$, where $\tau_c = (\gamma - \Gamma_0)/\omega_0^2$ is the characteristic time for the CDW segments to make a transition from oscillatory to diffusive motion.

Assuming that a certain number n^* of the conduction electrons are condensed into the fluctuating segments, and that these electrons have an effective mass m^*, we can use $M(t)$ and Eq. (7) to write a generalized complex conductivity

$$\hat{\sigma}^*(\omega) = \frac{n^* e^2}{m^*} \frac{\omega^2\Gamma - i\omega(\bar{\omega}_0^2 - \omega^2)}{(\bar{\omega}_0^2 - \omega^2)^2 + (\omega\Gamma)^2}, \quad (8)$$

where we have defined the frequency dependent resonance frequency and damping

$$\bar{\omega}_0^2(\omega) = \frac{(\omega\tau_c)^2}{1 + (\omega\tau_c)^2}\omega_0^2\ ,$$

$$\Gamma(\omega) = \Gamma_0 + \frac{\tau_c\omega_0^2}{1 + (\omega\tau_c)^2}.$$

For $\omega\tau_c \ll 1$, $\bar{\omega}_0 \to 0$ and $\Gamma \to \gamma$, and Eq. (8) reduces to the Drude result. In the opposite limit, $\omega\tau_c \gg 1$, $\bar{\omega}_0 \to \omega_0$ and $\Gamma \to \Gamma_0$, and σ^* takes the form of a Lorentz oscillator.

The low-frequency feature, which is evident for both $K_{0.3}MoO_3$ and $(TaSe_4)_2I$ can be fit with the real part of Eq. (8). We then compare the spectral weight of this contribution to that of the free electrons (given by the third and fourth terms of each fit in Tables II and III) in order to obtain the effective mass m^*. In this analysis we have estimated n^* from the reduction of the magnetic susceptibility,[8,10] which probes the electronic density of states at the Fermi level [$\chi = \mu_B^2 D(\mathcal{E}_F)$]. In the case of $K_{0.3}MoO_3$, ascribing the deviation of $\chi^{\rm spin}(300\ {\rm K}) = 21.1 \times 10^{-6}$ cm^3/mole from its unperturbed value $\chi^{\rm spin}(720\ {\rm K}) = \chi^{\rm Pauli} = 24.1 \times 10^{-6}$ cm^3/mole to condensation of a portion of charge carriers into the fluctuating CDW gives

$$\frac{n^*}{n_0} = 1 - \frac{\chi^{\rm spin}(T = 300\ {\rm K})}{\chi^{\rm Pauli}} = 0.13, \quad (9)$$

where n_0 is the total carrier concentration. In addition, we have added a Drude term to Eq. (8) in order to describe the contribution of the uncondensed electrons, and have used the same parameters as were used in the third term of the Drude-Lorentz fits (Tables II and III). Figure 9 shows such a fit to the low-frequency conductivity of $K_{0.3}MoO_3$ with the parameters given in Table IV. For $K_{0.3}MoO_3$ at 300 K, we find that the effective mass of the fluctuating electrons is $m^*/m_b = 95 \pm 15$, and at 200 K this increases to 240 ± 40, because $\chi^{\rm spin}(200\ {\rm K}) = 17.5 \times 10^{-6}$ cm^3/mole. This increase of the effective mass with decreasing temperature is in agreement with previous analysis[17] of only the FIR optical reflectivity at 200 K ($m^*/m_b = 170$), and with evaluations[39,45] of the low-temperature microwave conductivity ($m^*/m_b =$ 300–350). In addition, this feature also contributes to σ_1 only along the chain direction, with no evidence of such behavior perpendicular to the chains, i.e., it is a strictly one-dimensional effect.

For $(TaSe_4)_2I$, the Pauli susceptibility $\chi^{\rm Pauli}$ was found[8] to be 20.2×10^{-6} cm^3/mole, while $\chi^{\rm spin}(300\ {\rm K}) = 9.5 \times 10^{-6}$ cm^3/mole and $\chi^{\rm spin}(270\ {\rm K}) = 7.5 \times 10^{-6}$ cm^3/mole. Inserting these values into Eq. (9) yields $n^* = 0.53n_0$ at 300 K, consistent with the fact that the Peierls transition is significantly closer to room temperature in this material (Fig. 1). Again, using this and a fit to Eq. (8), the room-temperature mass enhancement of the condensed electrons is found to be $m^*/m_b = 2000 \pm 250$, increasing to 2800 ± 400 at 270 K because of the decrease of $\chi^{\rm spin}$ and the shifting of spectral weight. Again, this increase of the effective mass of the condensed electrons is in agreement with the result obtained[39,45] from low-temperature microwave conductivity measurements ($m^*/m_b \approx 10^4$).

This tendency of mass enhancement with decreasing temperature is also in accord with the mean-field expression[5,6,46] $m^*/m_e = 1 + \lambda^{-1}(2\Delta/\hbar\omega_{2k_F})^2$ relating

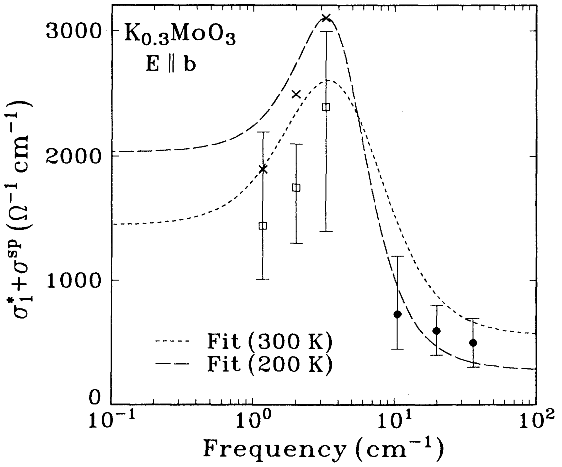

FIG. 9. Real part of the conductivity (dashed lines) calculated from Eq. (8), σ_1^*, plus a Drude term, $\sigma^{\rm sp}$, describing the response of the uncondensed electrons. Also shown are the measured conductivities of $K_{0.3}MoO_3$ at 300 K (open squares) and 200 K (crosses) by cavity perturbation, and at 300 K (solid circles) by Fabry-Pérot reflectivity, as described in the text.

TABLE IV. Parameters used to fit the low-frequency electrodynamic response of $K_{0.3}MoO_3$ and $(TaSe_4)_2I$ in the direction parallel to the chains using Eq. (8).

Material	Temp. (K)	ν_0 (cm^{-1})	ν_p (cm^{-1})	γ (cm^{-1})	Γ_0 (cm^{-1})
$(TaSe_4)_2I$	270	2	475	35	12
	300	3	450	30	12
$K_{0.3}MoO_3$	200	3	1000	9.5	4.5
	300	3	1030	20	8

m^* to the CDW energy gap Δ, where λ is the dimensionless electron-phonon coupling constant (somewhat less than one) and ω_{2k_F} is the phonon frequency of wave vector $2k_F$. Evaluation of this expression depends on the values chosen for Δ, ω_{2k_F}, and λ, but the results[45] are in good agreement with the measured values of m^* for both $K_{0.3}MoO_3$ and $(TaSe_4)_2I$. This mean-field relation between m^* and Δ also explains the significantly larger effective mass found in $(TaSe_4)_2I$ as compared to $K_{0.3}MoO_3$, given the larger CDW gap of the former (Table I).

Alloying of $K_{0.3}MoO_3$ smooths the Peierls transition, as seen in the dc conductivity [Fig. 2(b)] and causes a slight reduction in the absolute value of the room-temperature conductivity. From the comparison of the spectra in Fig. 8 we find that this is not due to an increase of the scattering rate since the narrow Drude-like feature has about the same width of 12 cm^{-1} in both compounds (cf. Table III). From the reduced spectral weight of this excitation (830 cm^{-1} compared to 1030 cm^{-1} for the pure sample, since $\nu_p^{\rm tot} = [(\nu_p^{\rm Drude})^2 + (\nu_p^{\rm ho})^2]^{1/2})$ it seems likely that the density of mobile condensed charge carriers is reduced compared to the pure material ($n^* = 0.10 n_0$), because an extra mass enhancement would not be expected for this small amount of dopant. This argument is supported by susceptibility measurements performed on pure and doped samples from the same batches used for our optical experiments.[38]

IV. CONCLUSION

We have presented a detailed study of the electrodynamic response of the one-dimensional conductors $K_{0.3}MoO_3$ and $(TaSe_4)_2I$ in an extremely wide spectral range. The experiments give clear evidence for important deviations from conventional metallic behavior in the fluctuating region, below $T^{\rm MF}$ but above $T_{\rm 3D}$, the temperature where long-range order develops. The frequency dependence of the conductivity in the direction parallel to the chains is characterized by a pseudogap, which develops below $T^{\rm MF}$, and also by a narrow excitation at low frequencies. Although the fluctuation regime exhibits a reduced electronic density of states at the Fermi energy (as seen in the spin susceptibility), collective contributions to the charge transport lead to an enhanced conductivity at low frequencies. Our results on the anisotropy clearly establish the collective mode aspect of the low-frequency conductivity and are evidence of interesting features such as a finite collective dc conductivity and a "quasipinned" response. These, together with the absence of a sharp Fermi edge as seen in photoemission experiments reported earlier,[23] are essential features of one-dimensional systems when correlations are important. It remains to be seen whether these experiments reflect simply the opening of a pseudogap, as suggested by the model of Lee, Rice, and Anderson,[1] or give evidence for non-Fermi liquid behavior, as predicted by the Luttinger model,[21,22] since both lead to a reduced density of states at the Fermi energy.

ACKNOWLEDGMENTS

V.V. Voitsekhovski provided the software for our analysis, which was done with the assistance of A. Pronin. Thanks to Yu. Goncharov for his aid with the submillimeter measurements. The U.S.-Russian collaboration is supported by NSF Grant No. 9216500. We also acknowledge the support of the Russian Research Foundation Grant No. 93-02-16110, of the Soros Foundation, and of NSF Grant No. 9218745. L.D. would like to thank the Swiss National Science Foundation for financial support of the U.S.-Swiss joint collaboration. M.D. would like to thank the Alexander von Humboldt Foundation for its support.

---

* Electronic address: schwartz@physics.ucla.edu

[1] P.A. Lee, T.M. Rice, and P.W. Anderson, Phys. Rev. Lett. **31**, 462 (1973).

[2] M.J. Rice and S. Strässler, Solid State Commun. **13**, 1389 (1973).

[3] D.J. Scalapino, Y. Imry, and P. Pincus, Phys. Rev. B **11**, 2042 (1975).

[4] H. Schultz, in *Low Dimensional Conductors and Superconductors*, edited by D. Jérôme and H.R. Caron (Plenum, New York, 1987).

[5] G. Grüner, Rev. Mod. Phys. **60**, 1129 (1988).

[6] G. Grüner, *Density Waves in Solids* (Addison-Wesley, Reading, MA, 1994).

[7] L.D. Landau and E.M. Lifshitz, *Statistical Physics* (Pergamon Press, London, 1959).

[8] D.C. Johnston, M. Maki, and G. Grüner, Solid State Commun. **53**, 5 (1985).

[9] D. Berner, G. Schreiber, A. Gaymann, H.M. Geserich, P. Monceau, and F. Lévy, J. Phys. (France) IV **3**, C2-255 (1993).

[10] D.C. Johnston, Phys. Rev. Lett. **52**, 2049 (1984).

[11] G. Travaglini, P. Wachter, J. Marcus, and C. Schlenker, Solid State Commun. **37**, 599 (1981).

[12] J.P. Pouget, S. Girault, A.H. Moudden, B. Hennion, C. Escribe-Filippini, and M. Sato, Phys. Scr. **T25**, 58 (1989); J.P. Pouget, B. Hennion, C. Escribe-Filippini, and M. Sato, Phys. Rev. B **43**, 8421 (1991).

[13] G. Travaglini, I. Morke, and P. Wachter, Solid State Com-

mun. **45**, 289 (1983).

[14] L. Degiorgi, S. Thieme, B. Alavi, G. Grüner, R.H. McKenzie, K. Kim, and F. Lévy, Phys. Rev. B **52**, 5602 (1995).

[15] J.P. Pouget and R. Comes, in *Charge Density Waves in Solids*, edited by L.P. Gor'kov and G. Grüner (North-Holland, Amsterdam, 1989).

[16] G. Travaglini and P. Wachter, Phys. Rev. B **30**, 1971 (1984).

[17] L. Degiorgi and G. Grüner, J. Phys. (France) I **2**, 523 (1992).

[18] H.P. Geserich, G. Schreiber, F. Lévy, P. Gressier, and P. Monceau, Mol. Cryst. Liq. Cryst. **121**, 19 (1985).

[19] H.P. Geserich, G. Schreiber, M. Dürrler, F. Lévy, and P. Monceau, Physica **143B**, 198 (1986).

[20] F. Wooten, *Optical Properties of Solids* (Academic Press, San Diego, 1972).

[21] H. Schultz, Int. J. Mod. Phys. B **5**, 57 (1991).

[22] S.P. Strong, D.G. Clarke, and P.W. Anderson, Phys. Rev. Lett. **73**, 1007 (1994).

[23] B. Dardel, M. Malterre, M. Grioni, P. Weibel, Y. Baer, and F. Lévy, Phys. Rev. Lett. **67**, 3144 (1991).

[24] B. Dardel, M. Malterre, M. Grioni, P. Weibel, Y. Baer, C. Schlenker, and Y. Pétroff, Europhys. Lett. **19**, 525 (1992).

[25] B.P. Gorshunov, A.A. Volkov, G.V. Kozlov, L. Degiorgi, A. Blank, T. Csiba, M. Dressel, Y. Kim, A. Schwartz, and G. Grüner, Phys. Rev. Lett. **73**, 308 (1994).

[26] M. Dressel, A. Schwartz, A. Blank, T. Csiba, G. Grüner, B.P. Gorshunov, A.A. Volkov, G.V. Kozlov, and L. Degiorgi, Synth. Met. **71**, 1893 (1995).

[27] D.S. Perloff, M. Vlasse, and A. World, J. Phys. Chem. Solids **30**, 1071 (1969); C. Schlenker, C. Filippini, J. Marcus, J. Dumas, J.P Pouget, and S. Kagoshima, J. Phys. (Paris) Colloq. **44**, C3-1757 (1983).

[28] O. Klein, S. Donovan, M. Dressel, and G. Grüner, Int. J. Infrared Millimeter Waves **14**, 2324 (1993).

[29] S. Donovan, O. Klein, M. Dressel, K. Holczer, and G. Grüner, Int. J. Infrared Millimeter Waves **14**, 2359 (1993).

[30] M. Dressel, O. Klein, S. Donovan, and G. Grüner, Int. J. Infrared Millimeter Waves **14**, 2389 (1993).

[31] A. Schwartz, M. Dressel, A. Blank, T. Csiba, G. Grüner, A.A. Volkov, B.P. Gorshunov, and G.V. Kozlov, Rev. Sci. Instrum. **66**, 2943 (1995).

[32] J.M. Ziman, *Principles of the Theory of Solids*, 2nd ed. (Cambridge University Press, Cambridge, 1972).

[33] A.A. Volkov, Yu.G. Goncharov, G.V. Kozlov, S.P. Lebedev, and A.M. Prokhorov, Infrared Phys. **25**, 369 (1985).

[34] A.A. Volkov, G.V. Kozlov, and A.M. Prokhorov, Infrared Phys. **29**, 747 (1989).

[35] A.A. Volkov, Yu.G. Goncharov, B.P. Gorshunov, G.V. Kozlov, A.M. Prokhorov, A.S. Prokhorov, V.A. Kozhevnikov, and S.M. Cheshnitskii, Fiz. Tverd Tela (Leningrad) **30**, 1718 (1988) [Sov. Phys. Solid State **30**, 988 (1988)].

[36] B.P. Gorshunov, Yu.G. Goncharov, G.V. Kozlov, A.M. Prokhorov, A.S. Prokhorov, and A.A. Volkov, Int. J. Mod. Phys. B **1**, 867 (1987).

[37] L. Degiorgi, B. Alavi, G. Mihály, and G. Grüner, Phys. Rev. B **44**, 7808 (1991); L. Degiorgi and G. Grüner, *ibid.* **44**, 7820 (1991).

[38] S. Brown (unpublished).

[39] S. Donovan, Y. Kim, B. Alavi, L. Degiorgi, and G. Grüner, Solid State Commun. **75**, 721 (1990).

[40] H. Mori, Prog. Theor. Phys. **33**, 423 (1965).

[41] R. Kubo, in *1965 Tokyo Summer Lectures in Theoretical Physics: Part 1, Many Body Theory*, edited by R. Kubo (Benjamin, New York, 1966).

[42] P. Brüesch, L. Pietronero, S. Strässler, and H.R. Zeller, Phys. Rev. B **15**, 4631 (1977).

[43] H.U. Beyeler, P. Büesch, L. Pietronero, W.R. Schneider, S. Strässler, and H.R. Zeller, in *Superionic Conductors*, edited by M.R. Salamon, Topics of Current Physics Vol. 15 (Springer, Berlin, 1979), p. 77.

[44] A.A. Volkov, G.V. Kozlov, S.P. Lebedev, and A.S. Rakitin, Fiz. Tverd Tela (Leningrad) **32**, 329 (1990) [Sov. Phys. Solid State **32**, 189 (1990)].

[45] T.W. Kim, D. Reagor, G. Grüner, K. Maki, and A. Virosztek, Phys. Rev. B **40**, 5372 (1989).

[46] P.A. Lee, T.M. Rice, and P.W. Anderson, Solid State Commun. **14**, 703 (1974).